Available online at www.sciencedirect.com
SCIENCE DIRECT
Journal of Colloid and Interface Science 300 (2006) 429–436
JOURNAL OF Colloid and Interface Science
www.elsevier.com/locate/jcis

Electroosmotically enhanced mass transfer through polyacrylamide gels

Marvi A. Matos [a], Lee R. White [a], Robert D. Tilton [a,b,*]

[a] *Center for Complex Fluids Engineering, Department of Chemical Engineering, Carnegie Mellon University, Pittsburgh, PA 15213, USA*
[b] *Department of Biomedical Engineering, Carnegie Mellon University, Pittsburgh, PA 15213, USA*

Received 24 February 2006; accepted 15 March 2006

Available online 18 March 2006

Abstract

We present an internal pumping strategy to enhance solute fluxes in polymer gels. The method is based on electroosmotic flow driven by an electric field applied across a gel that has been doped with charged colloidal inclusions. This work is motivated by the need to enhance the transport in gel-based biosensor devices whose response dynamics are often mass transfer limited. In this case, polyacrylamide gel slabs were doped with immobilized, charged silica colloids, and the flux of a fluorescent tracer was measured as a function of applied field strength, the volume fraction and size of the colloidal silica inclusions, and the bulk electrolyte composition. Significant flux enhancements were achieved with applied electric currents on the order of a few mA. Control experiments indicated that the flux enhancement was not due to any distortion of the gel diffusional properties in response to the presence of the inclusions. At a constant inclusion volume fraction, the electroosmotic solute flux enhancement was strongest for the smallest particle sizes that provide the highest total surface area, consistent with the electroosmotic mechanism whereby fluid flow is generated along the solid/liquid interface.

Keywords: Electroosmosis; Mass transport; Flux enhancement; Nanoparticles; Silica; Polyacrylamide; Crosslinked gels; Hydrogel; Particle immobilization

1. Introduction

Hydrogel matrices are commonly employed in DNA or protein electrophoresis and in biosensors [1–10]. Biosensor device designs often call for specific biomolecular recognition elements, such as enzymes, antibodies, lectins, or oligonucleotides to be immobilized in the sensor. Proteins have been successfully immobilized on flat [11,12] and spherical surfaces [13,14] and also inside gel matrices [15–17]. Although each of these immobilization schemes can result in functional biosensors, each has its own weaknesses. In the case of surface-immobilized proteins, suboptimal sensing arises due to protein deactivation or desorption [11,18]. Gel entrapment is less damaging to the protein. Polymeric networks also protect the proteins from possible proteolytic or microbial degradation and from fouling by cellular debris or other materials that may be present in crude samples.

The dynamics of any biosensor response to a change in analyte concentration are dictated by the coupling of mass transfer in series with the intrinsic biomolecular "sensing reaction." The use of polymer gel matrices introduces a stagnant zone between the sample and the active sensing elements that creates diffusion limitations [19–21], thereby slowing down the response rate. This limits the applicability of these sensors to single batch sample analyses or to continuously monitoring only processes whose dynamics are slow. Biosensors cannot be used to monitor dynamic processes whose timescales are shorter than the sensor response timescale. This has been problematic in cases where biosensors have been used to measure the rates of biomolecular association and dissociation reactions, where it has been reported that unaccounted mass transport limitations led to order of magnitude errors in rate constant determinations [22,23].

The potential to improve the performance of gel-based biosensors and similar devices motivates the development of appropriate strategies to promote mass transfer in gels. Electrophoresis has long been used to drive charged molecules through gels, and gel electrophoresis is a staple of molecular biology laboratories. Electrophoresis cannot serve as a generic

* Corresponding author.
E-mail address: tilton@andrew.cmu.edu (R.D. Tilton).

0021-9797/$ – see front matter
doi:10.1016/j.jcis.2006.03.036

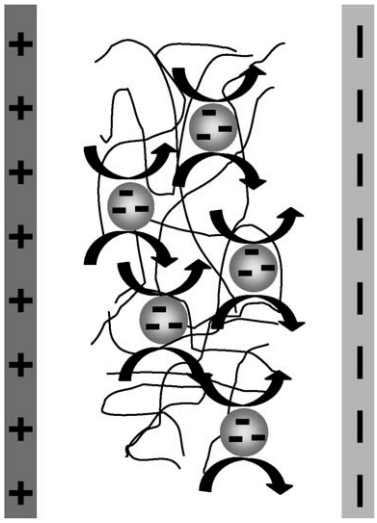

Fig. 1. Schematic view of electroosmosis for negatively charged silica colloids trapped inside a crosslinked gel. Application of an electric field across the gel exerts an electromotive force on counterions in the diffuse electrical double layers adjacent to the particle surfaces. This is transferred via viscous drag to a bulk flow of electrolyte solution parallel to the applied field direction.

tool for mass transfer enhancement, since it does not drive neutral molecules. The purpose of this paper is to demonstrate a novel internal pumping strategy based on electrically driven convection as a way to accelerate mass transfer of either charged or neutral molecules in polyacrylamide gels. The gels are doped with immobilized, charged colloidal inclusions that drive local electroosmotic flow in response to externally applied electric fields, as sketched schematically in Fig. 1.

Electroosmosis is the fluid motion induced by the electromotive force that acts on the unbalanced charge in the diffuse electrical double layer adjacent to a charged surface when an electric field is applied tangential to the surface. The electromotive force on the ions is transmitted to the fluid via viscous drag, resulting in bulk fluid flow that originates at the charged surface. This basic principle can be exploited to induce convection in biosensors where transport barriers otherwise suppress convection.

Here we demonstrate the feasibility of the electroosmotic internal pumping method and characterize its dependence on the size and volume fraction of the charged colloidal inclusions, the applied electric field magnitude and the electrolyte composition, using a fluorescent dye as a tracer to measure solute fluxes across gel slabs.

2. Experimental

2.1. Materials

All water was de-ionized by reverse osmosis and subsequently purified using ion exchange and carbon adsorption columns on a Milli-Q Plus system from Millipore. The fluorescent dye, amino-methylcoumarin ($\lambda_{ex} = 351$ nm, $\lambda_{em} = 430$ nm) was purchased from Invitrogen and used as received. The pK_a of this dye is 5. Silica nanoparticle samples, having 7 or 15 nm diameters, were obtained from Grace Davison. Stock silica suspensions at a weight fraction of 0.30 for the 7 nm particles and 0.40 for the 15 nm particles were dialyzed in de-ionized water before use. The electrophoretic mobility of these particles in 1 mM KNO_3 was measured using a Malvern Instruments Zeta-Sizer 3000 HS. The zeta potentials calculated from the mobilities [24] were -70 mV for both particle samples. KNO_3 was obtained from Sigma–Aldrich and used as received. D_2O used in neutron scattering experiments was used as received from Sigma–Aldrich.

Reagents for the polyacrylamide gel polymerization: acrylamide, N,N-methylene-bisacrylamide, ammonium persulfate and tetra-methylethylenediamine (TEMED) were obtained from Sigma–Aldrich and used as received. Aqueous stock solutions of acrylamide at a weight fraction of 0.25 and N,N-methylene-bisacrylamide at a weight fraction of 0.06, were prepared. A 0.1 g/mL solution of ammonium persulfate was made fresh before polymerization.

The weight fraction of acrylamide monomer before polymerization was 0.15 with a N,N-methylene-bisacrylamide crosslinker fraction of 0.04 (mass of crosslinker/mass of monomer). The weight fraction and crosslinker density were chosen to be sufficient to immobilize inclusions the size of proteins or larger inside the gel [25]. Before initiation, 6 mL of acrylamide stock solution and 1.0 mL of N,N-methylene-bisacrylamide stock solution were combined and mixed with a magnetic stir bar. Separate 3.5 mL portions of this solution were collected in different vials and mixed with 0.58 mL (for a final 0.02 particle volume fraction) of the 7 nm particle silica suspensions and 0.92 mL of de-ionized water and mixed thoroughly. The homogenized mixture was then degassed for 10 min at a gauge pressure of -80 kPa in a vacuum oven. A 75 μL aliquot of ammonium persulfate solution and a 15 μL aliquot of pure TEMED were mixed into 5 mL of each homogenized mixture before dispensing into an acrylic gel-holder using a microliter pipette. The gel holder, shown in Fig. 2, has an array of 2.68 mm diameter holes to support 29 individual gel columns that are polymerized simultaneously. To minimize air exposure during polymerization, this holder is sandwiched between an acrylic base and a glass slide. The reaction was allowed to proceed for 2 h.

The gels were stored in the aqueous solution of interest for at least 24 h before each experiment to ensure reproducible diffusion characteristics. After swelling in aqueous solution, the polymer fraction was approximately 0.13. These gel characteristics were previously found to be sufficient to entrap proteins having dimensions ∼3 nm [25], and therefore are appropriate to mimic a biosensor gel and also to immobilize 7 or 15 nm silica colloids.

2.2. Methods

2.2.1. Gel characterization

The effect of the colloidal inclusions on the polyacrylamide gel structure was investigated by small angle neutron scattering using the 30 meter SANS instrument NG3 at the National Institute of Standards and Technology in Gaithersburg, MD. A neutron wavelength of 6 Å was used with a spread $\Delta\lambda/\lambda$ of 0.15.

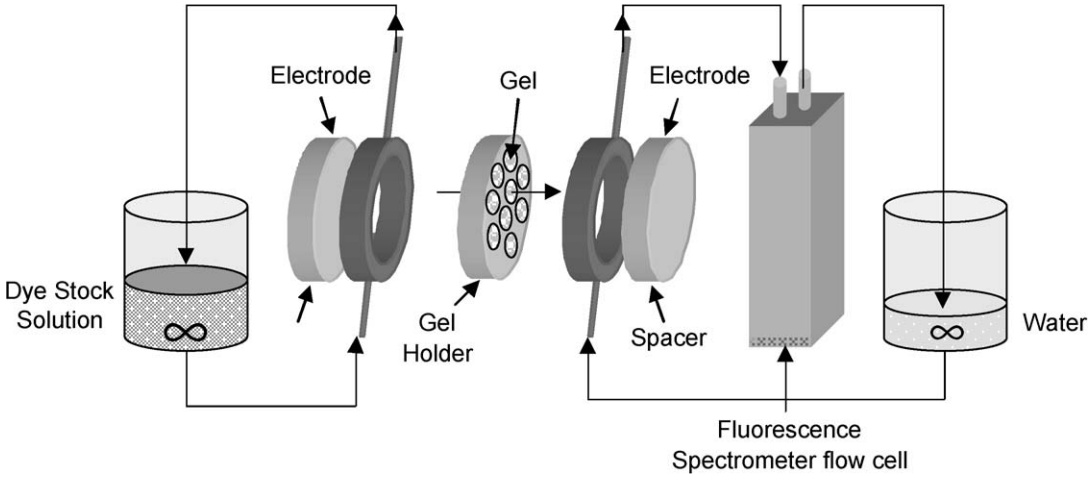

Fig. 2. Expanded schematic view of experimental apparatus for mass transport experiments. An acrylic gel holder supports 29 cylindrical gel columns measuring 2.68 mm in diameter and 1.68 mm in depth. Gold electrode disks are spaced 6 mm apart. Each contacts a 1.9 cm inner diameter double seal o-ring. A dye source solution is continuously pumped by a peristaltic pump past one side of the gel holder via two syringe needles injected through the o-ring and is recirculated to the reservoir. Similarly, a sink solution continuously flows past the opposite side of the gel holder, then through a fluorescence spectrometer and back to the sink solution reservoir. The sink and source flowrates are 8 cm^3/min. The source and sink total volumes are 50 and 10 mL, respectively.

Polymerized gel samples with and without particles, as well as dilute silica suspensions, were loaded in quartz cells. Using the open beam neutron flux the scattering profile was converted to an absolute scale. Incoherent background was subtracted from measurements at high wave vector values ($Q > 0.2$ Å^{-1}) [26]. All neutron scattering experiments were conducted with pure D_2O.

2.2.2. *Tracer flux measurements*

Fig. 2 provides a schematic view for the electroosmotic cell design. A pair of gold electrodes was placed parallel to the gel holder disk to produce a normal electric field. The gel holder separated two flow compartments served by a multi-channel peristaltic pump. The source compartment contained a continuously flowing solution of fluorescent tracer. The flow recirculated through a large reservoir that maintained a constant tracer concentration of 0.1 mM. The tracer that was transported across the gel was taken up in the sink compartment. The sink compartment consisted of a recirculating loop that took an initially tracer-free solution from a large reservoir, past the gel holder, then into a flow-through cuvette in a Spex Fluorolog 3-12 fluorescence spectrometer (Horiba-Jobin Yvon), and finally back into the sink reservoir.

The pH of the source and sink reservoirs were monitored throughout the experiment. The flow-through cuvette (Starna Cells, model 72F-Q-10) had a sample volume of 1.8 mL. The tracer source reservoir and the sink reservoir volumes were 50 and 10 mL, respectively, including the volume of the tubing. In each experiment, the tracer solution was made with the same electrolyte composition as the sink electrolyte solution. Before each experiment, the gel was rinsed profusely, mounted between the electrodes, and perfused with tracer free solutions on both sides of the compartment to equilibrate the gel before the start of each flux measurement. DC electric fields were produced by a Keithley 224 programmable current source and measured with an Agilent 34401A multimeter. All experiments were conducted at constant electric current.

The tracer flux measured using de-ionized water with no added salts was compared with the flux measured using 1 mM KNO_3 solution. Tracer concentrations in the sink solution were determined from the fluorescence intensity. Since aminomethylcoumarin fluorescence is pH-dependent, the tracer fluorescence intensity was calibrated as a function of concentration and corrected for pH.

3. Results and discussion

3.1. *Gel characterization*

Fig. 3 presents small angle neutron scattering results for gels polymerized with no silica particles, or gels containing either 7 or 15 nm particles at 2 vol%. Intensity data for aqueous suspensions of 7 and 15 nm silica particles at 0.5 vol% are also shown. The scattering intensity for spherical particles varies as a function of the scattering vector Q as:

$$I(Q) = C(\rho - \rho_s)^2 S(Q) P(Q), \tag{1}$$

where $I(Q)$, $S(Q)$ and $P(Q)$ are the scattering intensity, structure factor and form factor, respectively. The constant C is proportional to the concentration of particles, and $(\rho - \rho_s)$ is the difference between the particle and solvent scattering length densities [27]. The particle form factor $P(Q)$ was obtained from the scattering intensity for dilute suspensions of non-interacting particles. The scattered intensities for particle-loaded polyacrylamide gels were then normalized by $P(Q)$ in order to determine the structure factor $S(Q)$ (Fig. 3 inset). Comparing the scattering from the particle-free and particle-loaded gels shows the silica inclusions dominate the scattering in pure D_2O.

One concern with the design of the gel system was that polymerization might flocculate the silica particles, leading to

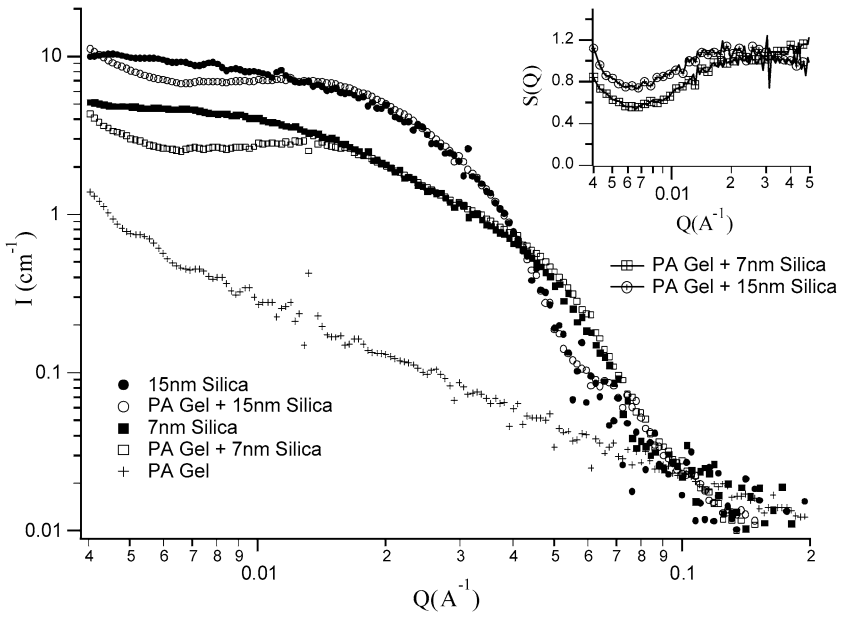

Fig. 3. Small angle neutron scattering from silica suspensions, polyacrylamide gels, and silica-laden polyacrylamide gels.

severely non-uniform particle distributions in the gel and inefficient mass transfer promotion as a result. Comparing the scattering intensity for gels with 7 or 15 nm silica particles with the scattering from the dilute silica suspensions indicates that silica particles did not aggregate during the gel polymerization. Particle aggregation leads to a power-law increase of scattering intensities in the low Q range ($Q \ll 2\pi/r$, where r is the particle radius) where the exponent is related to the fractal dimension [28–30]. The absence of fractal-like scattering is evidence that gel polymerization did not cause large-scale aggregation of the particles. However, the scattering does show significant structure factor effects. This indicates that particle–particle correlations were observed within the window of the scattering experiment.

Whereas the SANS data indicate that the silica particles were not aggregated, the appearance of a local minimum in $I(Q)$ and $S(Q)$ at $Q \sim 0.006$ Å^{-1} for the particle-laden gels suggests that the particle positions may be correlated in the gel. The form of $I(Q)$ for the free silica suspensions is the expectation for a dilute sample of uncorrelated spheres [31]. The low Q fringe in the particle-laden gel scattering suggests that there is a characteristic correlation distance between the particles. This distance appears to be from 30 to 60 nm for the 7 nm and the 15 nm particles.

3.2. Tracer flux

3.2.1. No external field

Tracer diffusion through the gel obeys the diffusion equation

$$\frac{\partial c}{\partial t} = D\frac{\partial^2 c}{\partial x^2} \tag{2}$$

subject to the following boundary conditions that are mandated by the continuous recirculation of both the source and sink compartments:

$$c(0,t) = C_{\text{source}}(0),$$

$$c(L,t) = C_{\text{sink}}(t) = \int_0^t \left[-D\frac{\partial c}{\partial x}(L,t)\right]\frac{A}{V}\,\mathrm{d}t, \tag{3}$$

where L, A and V are the thickness of the gel slab, the gel surface area exposed to solution, and the total volume of the recirculating sink compartment. The source compartment is sufficiently large that the tracer concentration remains constant at $C_{\text{source}}(0)$ and all mass transfer limitations are assumed to reside in the gel. Equations (2) and (3) are solved for $C_{\text{sink}}(t)$ at short times using Laplace transforms:

$$\begin{aligned} C(t) = {} & 2C_{\text{source}}(0)\operatorname{erfc}\left(\frac{1}{2}\frac{L}{D^{1/2}}t^{-1/2}\right) \\ & - \exp\left(\frac{LA}{V} + \left(\frac{AD^{1/2}}{V}\right)^2 t\right) \\ & \times \operatorname{erfc}\left(\frac{1}{2}\frac{L}{D^{1/2}}t^{-1/2} + \frac{AD^{1/2}}{V}t^{1/2}\right). \end{aligned} \tag{4}$$

Fig. 4 shows the accumulation of tracer in the sink compartment after diffusing through a particle-free polyacrylamide gel. Tracer concentrations are normalized as:

$$\frac{C_{\text{sink}}(t) - C_{\text{sink}}(0)}{C_{\text{source}}(0)(V_{\text{source}}/V_{\text{total}}) - C_{\text{sink}}(0)}, \tag{5}$$

where $C_{\text{sink}}(t)$ and $C_{\text{sink}}(0)$ are the concentrations measured in the sink compartment at time t and time 0. Fitting the tracer diffusion data to Eq. (4) indicates that the amino-methylcoumarin diffusion coefficient $D = 3.3 \times 10^{-6}$ cm^2/s in the polyacrylamide gel.

For control purposes, Fig. 5 compares the tracer diffusion across unfilled polyacrylamide gels against gels containing 2.0 vol% 7 nm silica particles, in the presence of either deionized water or 1.0 mM KNO_3. The presence of particles at 2.0 vol% had no effect on tracer diffusion through the gel, nor did the type of electrolyte medium. Similar results were obtained with 15 nm particles. Small differences in the mass

transport of dye across gels doped with 7 nm silica particles in 1 mM KNO_3 are attributed to experimental variability. Thus, the presence of silica inclusions had no effect on the structure of the gel that would impact mass transfer.

3.2.2. *Flux enhancement by applied dc fields: effects of particle size and concentration*

In all experiments with applied electric fields, the fields were applied 30 min after the start of each flux experiment. Thus, the first 30 min of each flux experiment correspond to simple diffusion. Inspection of this baseline flux was used to ensure that there were no variations in the intrinsic mass transfer properties of the gels before continuing to the measurement of electric field effects on mass transfer.

Fig. 6 presents results for tracer mass transfer across gel slabs under the application of dc fields in de-ionized water. For reference, the results for diffusion in the absence of an applied field are reproduced on this plot, and results are also presented for tracer transport through particle-free gels with an applied field. Particle-laden gels contain 2.0 vol% silica particles. An electrical current is denoted as positive when the cathode resides on the sink side of the gel slab, so the electroosmosis driven by the negatively charged inclusions forces solution from the source-side to the sink-side of the gel. A negative current drives electroosmosis toward the source-side.

First, note that tracer fluxes measured through particle-laden gels under the application of constant +3 mA dc currents are significantly enhanced relative to the simple diffusion flux. For comparison, the fluxes measured through particle-free gels with a +3 mA dc current are only slightly enhanced relative to the simple diffusion flux. The observation of a small flux enhancement under this condition indicates that ionic conduction ("electrophoresis") of the protonated fraction of the amino-methylcoumarin tracer ($pK = 5$) plays a small but finite role compared to the electroosmotic flux. The additional enhancement observed in the presence of silica inclusions indicates the

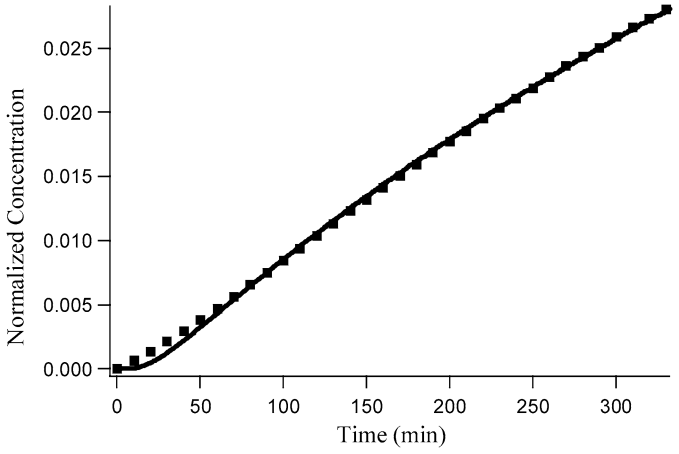

Fig. 4. The tracer accumulation in the sink solution during diffusion across the gel in the absence of an applied field is fitted to Eq. (4) to yield a tracer diffusion coefficient inside the gel of 3.3×10^{-6} cm^2/s.

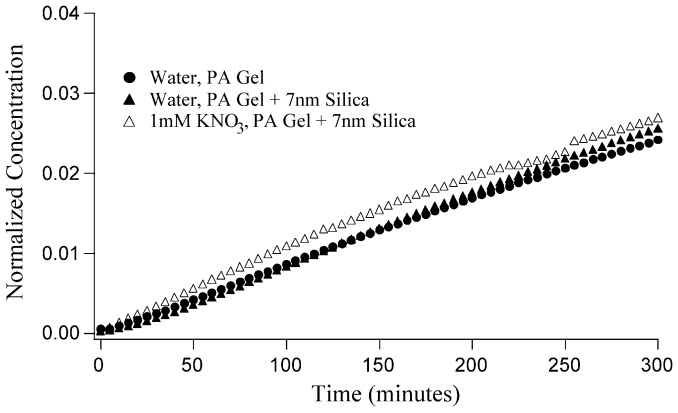

Fig. 5. Transport of amino-methylcoumarin through polyacrylamide gels with no externally applied electric field.

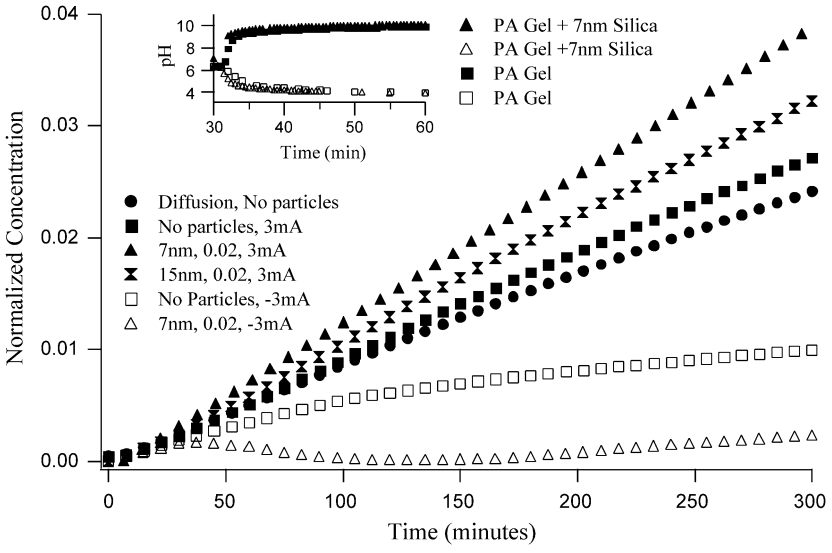

Fig. 6. Normalized sink concentration evolution for amino-methylcoumarin transport through 7 and 15 nm silica doped polyacrylamide gels and gels with no particles. No supporting electrolyte was used. DC electrical currents were applied 30 min after experiments started. Changing pH is monitored in the sink and source reservoirs as a function of time for gels with no particles and 7 nm silica doped gels with a current of 3 mA across the cell.

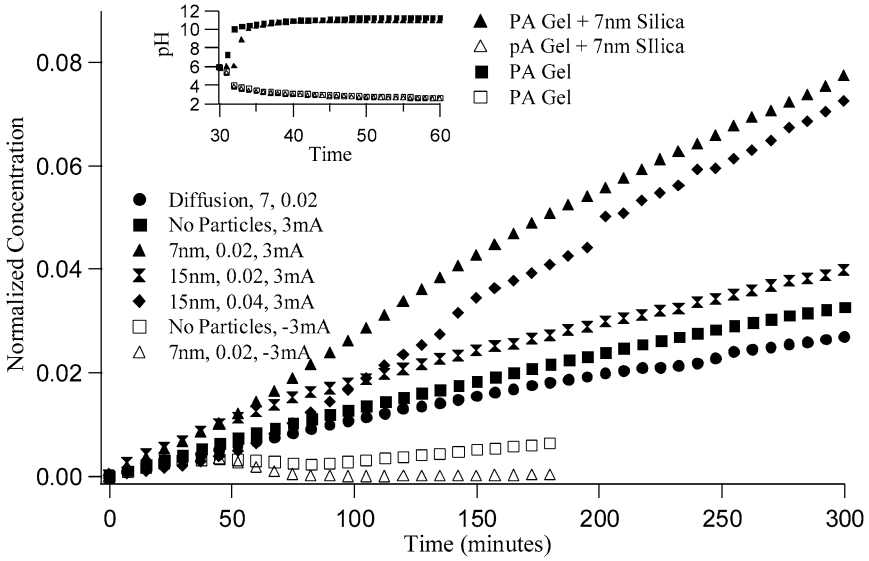

Fig. 7. Normalized sink concentration evolution for amino-methylcoumarin transport through 7 and 15 nm silica doped polyacrylamide gels at the indicated particle volume fractions and gels with no particles in the presence of 1 mM KNO_3. DC electrical currents are applied 30 min after the experiments started. Changing pH is monitored for both source and sink reservoirs.

contribution of a stronger electroosmotic enhancement on top of a weak electrophoretic contribution.

Fig. 6 also contains information about the effects of silica particle size on the electroosmotic flux enhancement. For a constant particle volume fraction of 2%, the 7 nm particles provide a greater enhancement than the 15 nm particles. The magnitude of the enhancement was quantified simply as the ratio of the normalized concentration achieved at the end of a 300 min experiment to that achieved at the end of 300 min of diffusion and electrophoresis through a gel without particles:

$$\text{Enhancement factor} = \frac{C_{\text{sink}}(\text{particles})}{C_{\text{sink}}(\text{no particles})}. \tag{6}$$

The enhancement factor was 1.19 ± 0.01 for the 15 nm silica particles and 1.44 ± 0.01 for the 7 nm silica particles (errors are based on repeated measurements). This is evidence that as the particle size decreases, at constant particle volume fraction, the electroosmotic pumping is more effective, due to the increased total surface area. This is explored further below.

Fig. 6 also shows that the tracer flux can be hindered, stalled or even transiently reversed, by the application of negative dc currents. Comparing particle-laden and particle-free gels for -3 mA current, the flux hindrance was more significant in the presence of particles, again indicating that the electroosmotic flux is stronger than the electrophoretic flux. The flux direction was transiently reversed from sink to source when -3 mA currents act on the gel that contains 2 vol% silica. This experiment also serves as a control against the possibility that the observed flux enhancements were an artifact of any electric field-induced damage to the gel that could have occurred, for example, if stresses arising from extended electric field application on the particle-laden gels may have created leaky channels for more rapid tracer transport. If the gels were simply made more permeable by some field-induced damage and there were no significant electroosmotic effect, the flux direction would not have reversed.

Electrolysis reactions during the prolonged dc electric field application produced a pH gradient across the gel. Measurements of pH in both flow compartments are shown in the inset of Fig. 6. The pH was constant during the first 30 min before the field was applied, but the pH in each compartment rapidly adjusted after the field application commenced at 30 min. This is to be expected, and similar effects have been noted with poly(ampholyte) gels and in microfluidic channels [32,33]. The pH gradients measured here were similar for particle-free and particle-laden gels.

Providing a background electrolyte provides more constant solution conductivity. This is addressed in Fig. 7. Compared to experiments conducted without added electrolytes, stronger electroosmotic flux enhancement was observed in the presence of 1.0 mM KNO_3 for 2.0 vol% silica gels under the action of $+3$ mA currents. The electroosmotic flux reversal with negative applied currents was also stronger than in the de-ionized water experiments. Although the pH gradient was larger in 1.0 mM KNO_3 than in de-ionized water, electrophoretic effects were still small compared to electroosmotic effects. The enhancement factor with 2.0 vol% of 15 nm particles was 1.21 ± 0.03 while 2.0 vol% 7 nm silica particles enhanced the flux by a factor of $\sim 2.36 \pm 0.03$.

Doubling the concentration of the 15 nm silica particles to 4.0 vol% produced a flux enhancement factor of 2.21, similar to that observed with 2.0 vol% of 7 nm silica particles. Since the area/volume ratio scales inversely with particle diameter, the total surface area of inclusions was the same for 2.0 vol% 7 nm silica and 4.0 vol% 15 nm silica. The scaling of flux enhancement with inclusion surface area is consistent with the fact that electroosmosis originates at the stationary solid–liquid interface.

Particle concentration effects were explored systematically for 7 nm silica particles in de-ionized water with constant $+3$ mA currents, as summarized in Fig. 8. The particle con-

centrations were 0.5, 1.0 and 2.0 vol%. Due to changes in the diffusive properties of the gel at greater than 2.0 vol% concentrations of 7 nm silica particles, concentrations exceeding 2.0 vol% were avoided. With an increasing number of particles in the system, more charged surface was available for electroosmotic pumping.

No significant enhancement was observed for 0.5 and 1.0 vol% concentrations. There appears to be a threshold in the particle volume fraction for enhancement of transport to occur, rather than a smooth dependence. A characteristic minimum average distance between the particles may be required before electroosmotic pumping is able to influence the tracer mass transfer. If the distance between inclusions is too great, viscous damping by the gel fibers will prevent the overlap of electroosmotic flows generated at distant particles and will lead to negligible overall mass transfer enhancement. Below a threshold inter-particle distance, flows generated at multiple inclusion sites will be additive and have a large net effect. If particles were arranged uniformly, the determination of this distance would be trivial. For 2 vol% 7 nm silica particles this average distance is ∼23 nm and for 2 vol% 15 nm silica particles, this distance is ∼50 nm. The SANS data do provide some additional insight, as the $S(Q)$ data suggest a characteristic separation distance on the order of 30–60 nm exists for both 7 and 15 nm silica particles.

3.2.3. Flux enhancement by applied dc fields: effect of applied electrical current

The effect of the applied current magnitude on the flux enhancement was measured in de-ionized water using 7 nm silica particles. The current was varied from 0 to 8 mA. Higher currents generated gas bubbles at the electrode surfaces and were avoided. As shown in Fig. 9, the dependence of the tracer flux on current magnitude is non-linear. In de-ionized water, significant flux enhancement was observed with currents as low as +0.25 mA.

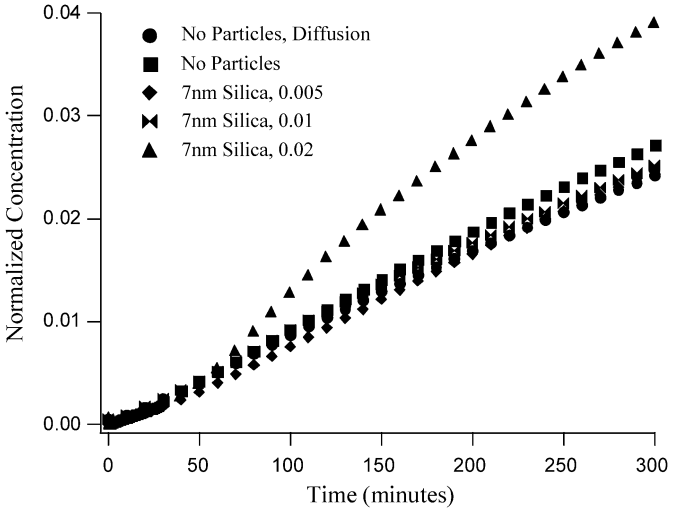

Fig. 8. Normalized sink concentration evolution for amino-methylcoumarin transport through 7 nm silica doped polyacrylamide gels and gels with no particles in water. Particle concentrations of 0.5, 1.0 and 2.0 vol% were used. 3 mA dc currents were applied 30 min after the experiments started.

The effect of pH on the relative contributions of electroosmosis and electrophoresis is important. Under acidic conditions, electrophoresis of positively charged amino-methylcoumarin occurs in parallel with the electroosmotic convection around the charged silica particles. Under basic conditions, electrophoresis is negligible. The magnitude of the pH gradient generated by the applied current depends on the electrolyte composition. The generation of H^+ ions at the electrode on the source-side of the gel results in low pH, tracer charging, and possible tracer electrophoresis on that side of the gel. The generation of OH^- ions at the electrode on the sink side neutralizes the tracer on that side of the gel. On the basic sink-side of the gel, there is no electrophoresis, only diffusion and electroosmosis.

Another effect of the pH gradient is the strong localization of the electric fields as shown schematically in Fig. 10. The concentration of H^+ ions is high (pH ∼ 3) in the source side and

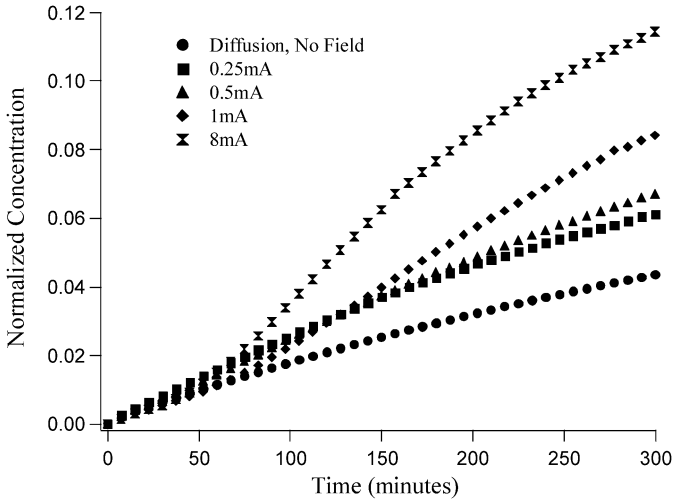

Fig. 9. Normalized sink concentration evolution for amino-methylcoumarin transport through 7 nm silica doped polyacrylamide gels in water with a 0.02 particle volume fraction. DC currents of 0.25, 0.5, 1.0 and 8.0 mA, were applied 30 min after the experiments started.

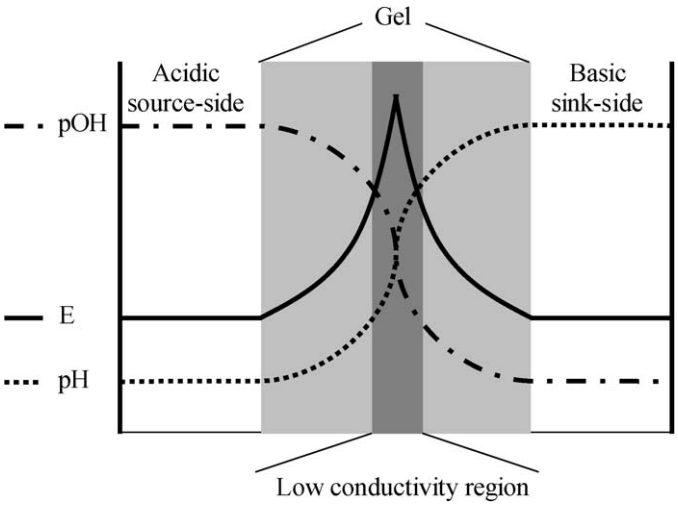

Fig. 10. Schematic view of pH gradient and electric field profile across polyacrylamide gels as a result of applied DC currents.

low (pH $\sim$ 11) in the sink side. The opposite is true for OH^- (pOH $\sim$ 3 on the sink side and $\sim$11 on the source side). Ions must cross the gel and the medium conductivity is decreased in the middle of the gel, where the pH = pOH = 7 due to the neutralization of the H^+ and OH^-. Thus, the ionic concentration in the neutral middle of the gel is $\sim$4 orders of magnitude lower than it is in the outer regions of the gel. Because the conductivity is low here, the electric field magnitude must be higher in the middle of the gel than in the outer region for the constant current conditions used in these experiments. Electroosmosis is most effective in that high field region, where electrophoresis is also negligible, due to the local pH exceeding the pK_a of amino-methylcoumarin. Note that this effect would be diminished by adding higher concentrations of indifferent electrolytes that would maintain a more constant conductivity across the gel.

4. Summary

Polyacrylamide gels can be prepared with silica nanoparticle inclusions at concentrations of 2.0 vol% and less, with no significant effect on amino-methylcoumarin tracer diffusivities. Under applied electric fields the mass transport of amino-methylcoumarin is enhanced in particle-laden polyacrylamide gels, mainly due to the generation of electroosmotic flows around the charged inclusion surfaces. For a constant inclusion volume fraction, the electroosmotic flux enhancement is greater for smaller particles than larger particles, owing to the greater total surface area. The scaling of flux enhancement with total surface area is consistent with the generation of an electroosmotic slip at the particle surfaces. By reversing the direction of the applied electrical current, the electroosmotic flow can be used to hinder or suppress tracer mass transfer through the gel. The ability to use electroosmosis, rather than electrophoresis alone, is significant in that it has the potential to drive mass transfer of neutral solutes through gels. This may have applicability for tools to promote mass transfer and mixing in gel-based biosensors or other biomedical devices.

Acknowledgments

This work is made possible by NASA research Grant NAG8-1842. The authors would like to thank Dr. Yuri Solomontsev for insightful conversations during the early stages of this research.

References

[1] P.P. Joshi, S.A. Merchant, Y.D. Wang, D.W. Schmidtke, Anal. Chem. 77 (2005) 3183.
[2] E. Fernandez, D. Lopez, E. Lopez-Cabarcos, C. Mijangos, Polymer 46 (2005) 2211.
[3] V.K. Yadavalli, W.G. Koh, G.J. Lazur, M.V. Pishko, Sens. Actuators B: Chem. 97 (2004) 290.
[4] X.J. Wu, M.M.F. Choi, Anal. Chem. 75 (2003) 4019.
[5] Y. Chevalier, L. Coche-Guerente, P. Labbe, Mater. Sci. Eng. C: Biomim. Supramol. Systems 21 (2002) 81.
[6] S. Brahim, D. Narinesingh, A. Guiseppi-Elie, Biosens. Bioelectron. 17 (2002) 53.
[7] S.I. Brahim, D. Maharajh, D. Narinesingh, A. Guiseppi-Elie, Anal. Lett. 35 (2002) 797.
[8] R.J. Russell, M.V. Pishko, C.C. Gefrides, M.J. McShane, G.L. Cote, Anal. Chem. 71 (1999) 3126.
[9] A.L. Crubliss, J.G. Stonehuerner, R.W. Henkens, J. Zhao, J.P. Odaly, Biosens. Bioelectron. 8 (1993) 331.
[10] B. Linke, W. Kerner, M. Kiwit, M. Pishko, A. Heller, Biosens. Bioelectron. 9 (1994) 151.
[11] E.F. Tsung, R.D. Tilton, J. Colloid Interface Sci. 213 (1999) 208.
[12] N. Xia, Y.H. Hu, D.W. Grainger, D.G. Castner, Langmuir 18 (2002) 3255.
[13] D.L. Graham, H. Ferreira, J. Bernardo, P.P. Freitas, J.M.S. Cabral, J. Appl. Phys. 91 (2002) 7786.
[14] G.H. Seong, J. Heo, R.M. Crooks, Anal. Chem. 75 (2003) 3161.
[15] C. Kurzawa, A. Hengstenberg, W. Schuhmann, Anal. Chem. 74 (2002) 355.
[16] E.L. Cabarcos, B.J.R. Retama, B.L. Ruiz, M. Heinrich, A.F. Barbero, Physica A: Statistical Mechanics and Its Applications 344 (2004) 417.
[17] S. Basu, P.J. Campagnola, Biomacromolecules 5 (2004) 572.
[18] L. Joss, T.A. Morton, M.L. Doyle, D.G. Myszka, Anal. Biochem. 261 (1998) 203.
[19] W.R. Vieth, Membrane Systems Analysis and Design: Applications in Biotechnology, Biomedicine, and Polymer Science, Wiley, New York, 1988.
[20] G. Ramsey, Chemical Analysis, vol. 18, Wiley, New York, 1998.
[21] D. Diamond, Principles of Chemical and Biological Sensors, Chemical Analysis, Wiley, New York, 1998.
[22] P. Schuck, A.P. Minton, Anal. Biochem. 240 (1996) 262.
[23] P. Schuck, Biophys. J. 70 (1996) 1230.
[24] R.W. Obrien, L.R. White, J. Chem. Soc., Faraday Trans. II 74 (1978) 1607.
[25] J. Tong, J.L. Anderson, Biophys. J. 70 (1996) 1505.
[26] C.J. Glinka, J.G. Barker, B. Hammouda, S. Krueger, J.J. Moyer, W.J. Orts, J. Appl. Crystallogr. 31 (1998) 430.
[27] A. Guinier, Small-Angle Scattering from X-Rays, Wiley, New York, 1955.
[28] B. Knoblich, T. Gerber, J. Non-Cryst. Solids 283 (2001) 109.
[29] F. Saint-Michel, F. Pignon, A. Magnin, J. Colloid Interface Sci. 267 (2003) 314.
[30] T.P. Rieker, S. Misono, F. Ehrburger-Dolle, Langmuir 15 (1999) 914.
[31] W.L. Griffith, R. Triolo, A.L. Compere, Phys. Rev. A 35 (1987) 2200.
[32] S.E. Kudaibergenov, V.B. Sigitov, A.G. Didukh, S.B. Moldakarimov, Abst. Pap. Am. Chem. Soc. 219 (2000) U444.
[33] A.R. Minerick, A.E. Ostafin, H.C. Chang, Electrophoresis 23 (2002) 2165.